# Three-dimensional Structure of Actin Filaments and of an Actin Gel Made with Actin-binding Protein

RICHARD NIEDERMAN, PHILIP C. AMREIN, and JOHN HARTWIG
*Hematology-Oncology Unit, Department of Medicine, Massachusetts General Hospital, Boston, Massachusetts 02114; and the Veterans Administration Medical Center, West Roxbury, Massachusetts 02132*

ABSTRACT Purified muscle actin and mixtures of actin and actin-binding protein were examined in the transmission electron microscope after fixation, critical point drying, and rotary shadowing. The three-dimensional structure of the protein assemblies was analyzed by a computer-assisted graphic analysis applicable to generalized filament networks. This analysis yielded information concerning the frequency of filament intersections, the filament length between these intersections, the angle at which filaments branch at these intersections, and the concentration of filaments within a defined volume. Purified actin at a concentration of 1 mg/ml assembled into a uniform mass of long filaments which overlap at random angles between 0° and 90°. Actin in the presence of macrophage actin-binding protein assembled into short, straight filaments, organized in a perpendicular branching network. The distance between branch points was inversely related to the molar ratio of actin-binding protein to actin. This distance was what would be predicted if actin filaments grew at right angles off of nucleation sites on the two ends of actin-binding protein dimers, and then annealed. The results suggest that actin in combination with actin-binding protein self-assembles to form a three-dimensional network resembling the peripheral cytoskeleton of motile cells.

The recent interest of cell biologists in the interactions of actin filaments with one another is based on the finding that the cortical cytoplasm of many eukaryotic cells contains an actin filament network. The structural relationship between actin filaments responsible for their mechanical properties is potentially discernible in the electron microscope, a possibility supported by increasingly improved images of the three-dimensional structure of macromolecular assemblies, including those within cells (13, 14, 22–25, 33). Studies of the mechanical properties of actin filaments, both in purified state and in the presence of proteins that modulate their mechanical behavior, is beginning to yield a molecular picture of the nature of these interactions, views which are reviewed in references 20 and 28. The three-dimensional relationships of actin filaments observed in the electron microscope, together with rheological measurements, can provide a complete picture of the molecular basis for the mechanical properties of actin networks. This picture would provide a basis for making mechanical interpretations of actin filament networks observed with the electron microscope.

As a step in the direction of analyzing the three-dimensional structure of actin networks, we have developed a computer program for determining four parameters of filament networks from stereoscopic images obtained in the electron microscope. These parameters are: (*a*) the frequency of filament overlaps; (*b*) the distance between the overlaps; (*c*) the angles of overlap; and (*d*) the mass of filaments in a defined volume. This paper describes these properties for purified actin filaments and for actin assembled in the presence of macrophage actin-binding protein.

## MATERIALS AND METHODS

Actin, prepared from rabbit skeletal muscle by the method of Spudich and Watt (26), was further purified by column chromatography on Sephadex G-150 (11). Macrophage actin-binding protein was prepared as described previously (11). Purified actin, 1 mg/ml, or actin mixed with various concentrations of actin-binding protein was polymerized on electron microscope grids attached to glass slides. The grids (200 mesh, Pelco, Tustin, CA) were coated sequentially with: 0.25% Formvar by evaporation from ethylene dichloride; 1% polylysine ($M_r$ 20,000, Sigma Chemical Co., St. Louis, MO); and finally 1% bovine serum albumin at 1 mg/ml (Sigma Chemical Co.). The grids were washed thoroughly



THE JOURNAL OF CELL BIOLOGY · VOLUME 96 MAY 1983 1400–1413

with deionized distilled water after being coated with the albumin solution, and allowed to dry until use. Actin, in a solution containing 0.2 mM $CaCl_2$, 0.5 mM ATP, 0.5 mM 2-mercaptoethanol, and 2 mM Tris-HCl, pH 7.5 was mixed with various concentrations of actin-binding protein in the same solution. The actin was polymerized by the addition of KCl and $MgCl_2$ to final concentrations of 100 mM and 2 mM, respectively. 10 μl of the protein solution was placed on each grid and incubated in moistened petri dishes at room temperature. After 30 min the slides and adherent grids were placed in a solution containing 60 mM PIPES, 40 HEPES, 10 mM EGTA, 2 mM $MgCl_2$ (PHEM buffer of Schliwa and Van Blerkom [24]). The grids were fixed with 1% glutaraldehyde (Pelco) diluted from an 8% stock solution in PHEM buffer for 10 min at room temperature. After fixation the grids were dipped in PHEM buffer, then placed in 0.5% $OsO_4$ in PHEM buffer for 5 min. They were then: dehydrated through increasing concentrations of ethanol; critical-point-dried from ethanol with liquid $CO_2$ (1); rotary shadowed with plantinum-carbon at 25° (13, 17); and then viewed in a Philips 301 electron microscope at an accelerating voltage of 60 keV. Stereo pair photographs were taken at ±6° (7, 8).

*Morphometry:* Stereo pair electron micrographs of the actin and actin-binding protein gels were magnified 150,000 times to carry out the morphometric analyses. Enlarged pairs of photographs were placed on the graphics tablet of an Apple II + microcomputer equipped with a floppy disk (Apple Computer, Inc., Cupertino, CA). The graphics tablet was placed on a 9 × 9 inch stereo viewer (Polysciences, Inc., Warrington, PA). Stereo photographs were taped onto the graphics tablet and aligned vertically and horizontally. Verticality was determined by the axis of tilt in the microscope by taking double exposures of the same specimen moved parallel to the axis of tilt. Horizontality was established by aligning a given object in both photographs in the same horizontal plane. This procedure gave the appearance of three dimensions when viewed through the stereo viewer. The scale of graphics tablet was calibrated by entering two points defining a known distance between them at the final magnification of the photographs. A reference point was designated in each picture for calculating distances to all other points subsequently entered into the computer (for detailed sample calculation, see page 1409 and Fig. 2). All filaments within a viewing area were entered to the computer. Filament segments were entered by sequentially placing the pen of the graphics tablet on an identical feature of the same filament in each micrograph. The *X*, *Y*, and *Z* coordinates of the entered points were determined by the computer. Filaments were defined as vectors running between two points entered sequentially (see Appendix).

The following four parameters were established and measured: (*a*) filament overlaps or intersections, (*b*) the angles formed by intersecting filaments, (*c*) filament length between intersections, and (*d*) the concentration of actin filaments in a defined volume.

FILAMENT INTERSECTIONS: Filaments often appeared to overlap one another when viewed in stereo. Three types of intersections were observed: filaments that clearly ended by intersecting a second filament along its length (T junctions); filaments that crossed other filaments (X junctions); and filament junctions involving more than two filaments (foci). The validity of apparent *T*, *X*, and focal intersections was established with the computer. Identical points on each of the two filaments involved in the intersection were entered with the graphics pen. The points on the filaments were picked such that they were on opposite sides of the apparent intersection. For these intersections, the computer calculated the distance between the crossing filaments. If the distance was calculated to be ≤10 nm, the filaments were judged to intersect. This distance was the diameter of single actin filament as detailed in Results. Although T-junctions could be easily discerned by viewing in stereo, these intersections were validated by the same method except that the end of the filament forming the T was entered as no filament existed on the opposite side of the junction.

INTERSECTION ANGLE: If the filaments were determined to intersect as detailed above, the angle formed at the intersection was calculated.

FILAMENT LENGTH BETWEEN INTERSECTIONS: The filament length between valid intersections was measured. The graphics pen was placed on the vertices of the two junctions and the length between these points was determined.

CONCENTRATION OF ACTIN FILAMENTS: The concentration of actin in 0.5 to 0.75-$\mu m^3$ volumes was calculated by summing the lengths of all filaments within the volume (see Appendix) and converting this sum to mg/ml by the expression: filament length/ml × 370 molecules/μm × 42,000 g/mol $6.023 \times 10^{20}$ molecules/mol.

## RESULTS

In the experimental results described below, we examined two structural features. First, we surveyed the overall appearance of the protein assemblies on the grid. Second, we examined the detailed structure of these protein assemblies within a defined region of the grid.

### *Three-dimensional Structure of Purified Actin Filaments*

When a 1-mg/ml solution of actin was polymerized on the surface of a grid by the addition of a KCl, filaments were found to distribute relatively evenly over the grid surface. Fig. 1 is an electron micrograph displaying the appearance of the actin at low magnification.

Single filaments have a 10-nm diameter and in many cases the 37-nm periodicity of the actin filaments is preserved (Fig. 2). The structure of actin revealed by this technique is therefore similar to that in negatively stained actin preparations, except that the filaments appeared wider, and the three-dimensionality of the solutions appears to be preserved.

The apparent homogeneous distribution of actin over the grid surface was established quantitatively by analyzing the concentration of actin in random regions of micrographs. The actin concentration calculated from the micrographs ranged between 0.5 and 1.5 mg/ml in 0.75-$\mu m^3$ volumes analyzed. In many cases, what appeared to the eye as differences in the apparent filament concentration was due to variations in the depth of field. Three-dimensional viewing of stereo pairs revealed that the filaments were relatively straight and tended to be >1.5 μm in length. Some of them overlapped and others aligned side-to-side (Fig. 2). With the assistance of the computer analysis it was possible to ascertain with confidence when filaments made contact with one another. The average distance between filament contacts was 0.70 ± 0.38 μm (mean ± SD). This number is a minimal estimate of the spacing between filament contacts, because the maximum length of filaments that could be measured in the viewing field was ~1.5 μm. In other words, at the magnification used, most filaments ran off of the micrographs at both ends but intersected at least one other filament as it crossed the micrograph.

### *Three-dimensional Structure of Actin Assembled with Actin-binding Protein*

When actin was polymerized with actin-binding protein at molar ratios of 50:1 and 25:1 (actin/actin-binding protein), its arrangement on the grid was different from that of actin alone. Fig. 3 is a low magnification electron micrograph of actin assembled in the presence of actin-binding protein. In contrast to actin, the distribution of actin plus actin-binding protein was discontinuous on the grid. Filament aggregates were randomly distributed across the grid and were separated by areas either lacking or sparsely covered with filamentous material (Fig. 3). The filament aggregates were of variable size, and many of them covered relatively large areas of the grid (Figs. 4–6). These regions are designated as "network densities." Despite the local variation in filament density, the structure of filaments appears to be similar in both regions of high and low filament concentration.

In detailed structure, the network densities were also entirely different from pure actin. First, the actin concentration in the densities was much higher than that of pure actin, and ranged from 6 to 12 mg/ml in volumes analyzed, despite the fact that nearly identical actin concentrations had been applied to the grids in both cases. Second, the filaments were short, straight, and highly branched. Third, the distances between actin filament intersections in the network densities were much shorter than was observed in purified actin. The measured length between the filament intersections was related to the amount of actin-binding protein present during the assembly process

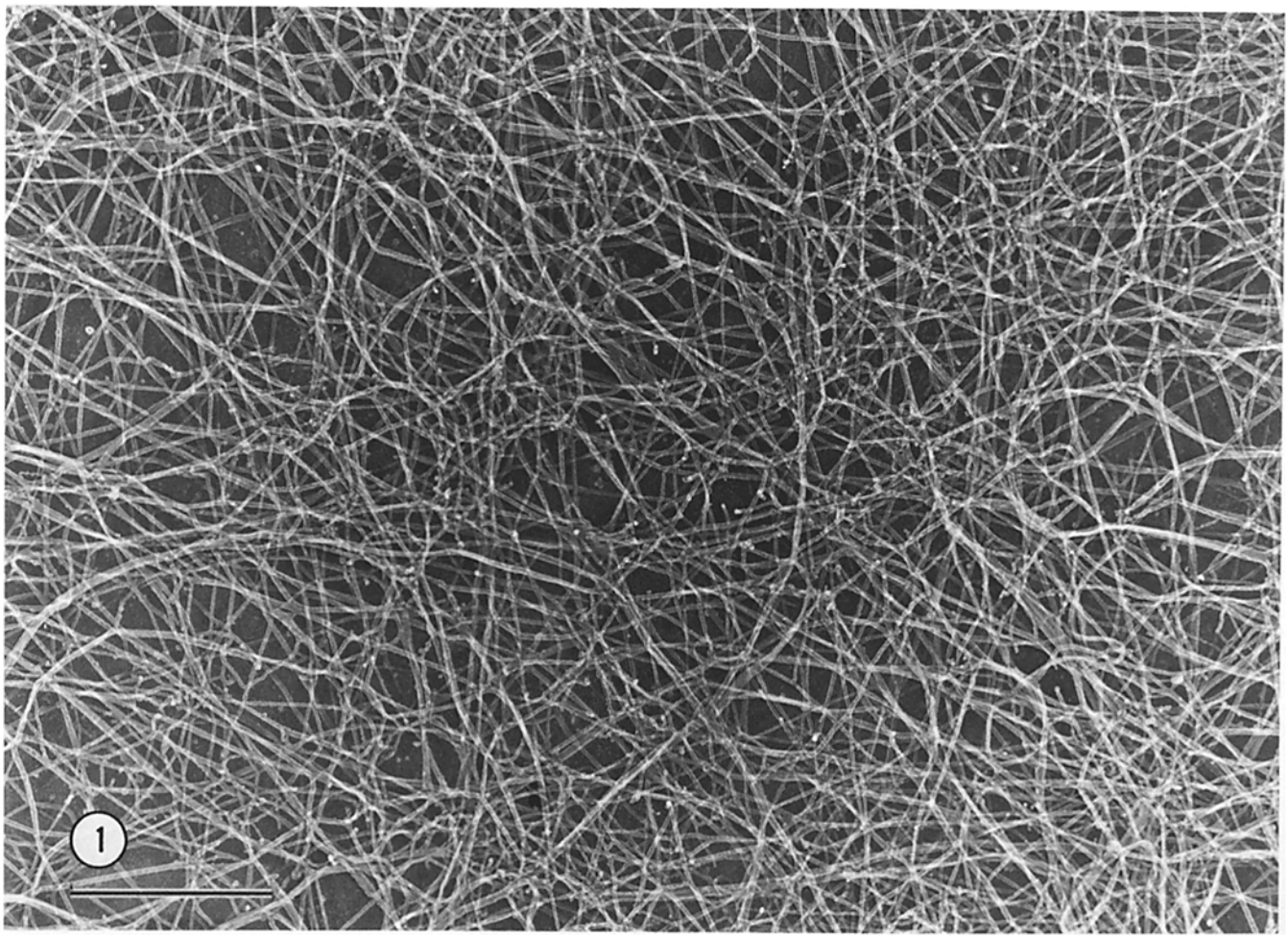


FIGURE 1 Low magnification electron micrograph of actin, 1 mg/ml, polymerized on the surface of a grid and then processed as described in Methods. The average actin concentration determined from five different areas in stereo micrographs of this photograph was 1.43 mg/ml. Bar, 1 μm. × 28,000.

(Fig. 7). At a molar ratio of 1 actin-binding protein to 50 actin monomers, the mean intersection length between filaments was 165 ± 100 nm. At higher molar ratios of actin-binding protein to actin (1:25), the perpendicular branching morphology remained, but the network spacing was shortened. The mean length between filament intersections was reduced to 103 ± 50 nm (compare Figs. 4 and 5).

Two types of filament intersections, either X- or T-shaped, are revealed in high magnification stereo electron micrographs (Fig. 6). The most common type of branching encountered was X-shaped. The angle of branching from X- and T-intersections was always near perpendicular (Fig. 7). More than 70% of the filaments crossed within 20° of perpendicular. This perpendicular branching of actin did not depend on the local actin concentration, since areas of lower concentration on the grid, away from the densities, also displayed the same perpendicularity.

## DISCUSSION

This paper provides quantitative information about the structure of actin and of an actin gel formed by macrophage actin-binding protein. Actin assembled in the presence of actin-binding protein forms a perpendicularly branched network of short, straight filaments. The structure of this network is strikingly different from that of actin alone. However, the structure is quite similar to the cortical actin network as visualized in electron micrographs of various motile cells (2, 13, 23–25, 33).

### *Actin*

Actin on grids existed as a continuous mat of long, relatively straight filaments. Filaments made contact on average once every 0.7 μm, at angles varying continuously between 0° and 90°. This three-dimensional organization seems to be representative of F-actin in solution because the average concentrations of actin determined across the grid by computer analysis of micrographs was near that actually applied. Although the micrographs provide no direct information as to the chemical nature of interactions at the filament junctions, rheologic data are most consistent with the conclusion that purified actin filaments in 0.1-M KCl solutions in vitro are long, extensively overlapping semiflexible polymers, and that the impediments to diffusion imposed by these overlaps account for the high viscosity of purified F-actin (29, 36). Furthermore, the stress required to disentangle these filaments is extremely low (28, 35, 36), indicating that there are no specific chemical bonds at the junctions.

### *Actin Assembled with Actin-binding Protein*

Actin assembled in the presence of actin-binding protein acquires mechanical properties resembling those of a gel (5, 27,

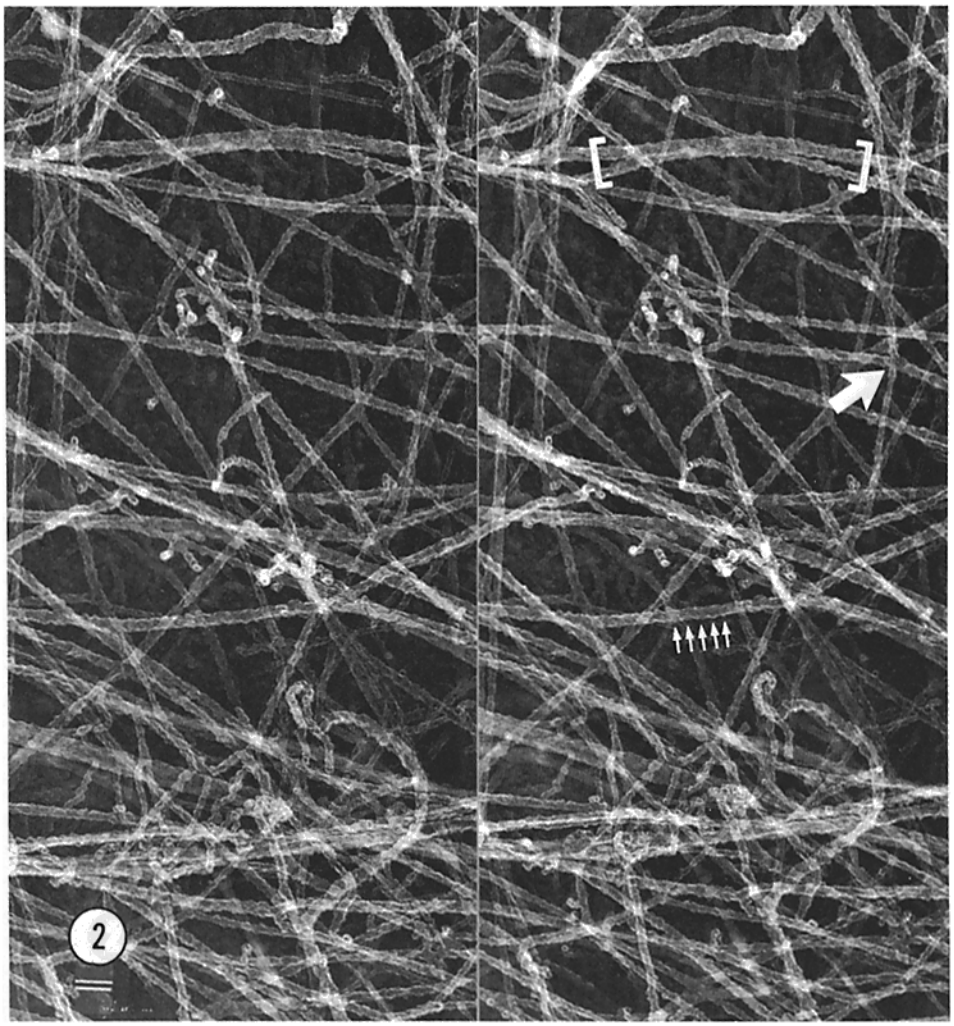

FIGURE 2 Stereo electron micrographs of purified F-actin. Actin filaments are several microns long and can be seen to overlap or cross one another (large arrows) and lie side by side (brackets) at a number of points. The filaments exhibit a helical twist and occasionally a 37-nm axial repeat (small arrows). The actin concentration is 0.5 mg/ml. Tilt is ±6°. Bar, 1 μm. × 50,000.

28), the rigidity of which is proportional to the concentration of actin-binding protein added (28). The data presented here suggest that a 1-mg/ml solution of actin assembled with actin-binding protein in molar ratios of 50 or 25 actin monomers to 1 actin-binding protein molecule forms discontinuous structures over the grid surface. However, despite this difference in gross appearance, the fine structure of the filaments was similar in both regions of high and low concentrations. Filaments are short, straight, and branch at 90° angles.

Actin-binding protein promotes the perpendicular alignment of actin filaments (12). Random cross-linking of flexible polymer chains can easily form an isotropic network, but the random cross-linking of straight, relatively stiff actin polymers tends to align the filaments in parallel (9). For example, several proteins that cross-link actin filaments promote bundling of the actin filaments (3, 4, 6, 10). In contrast, the perpendicular branching of actin by actin-binding protein increases the isotropy of the actin filaments by *preventing* bundle formation (11).

Actin-binding protein molecules nucleate actin assembly. The polarity of the actin filaments at these intersections was previously defined by labeling of the filaments with the heavy meromyosin subfragment of myosin. The arrowheads pointed toward the elbows of the intersection. This orientation is consistent with filament assembly beginning at the branch points. The "barbed" filament's end is therefore farthest from the elbow. Therefore, actin filaments initially grow off actin-binding protein nuclei in the "preferred" direction (21, 34) forming short L-shaped structures. These structures have the "unpreferred" end of the original nuclei near the point where the filaments cross (12).

Three mechanisms for joining these branching structures into a continuous network are possible: (*a*) annealing of the filaments; (*b*) monomer exchange from the short to longer filaments; or (*c*) free molecules of actin-binding protein linking network segments. The simplest explanation for the structure of this self-assembling system is depicted in Fig. 8. Assembly is a three-step process: (*a*) Short branches form as described above. (*b*) Subsequent growth of the nucleated filaments in the "nonpreferred" direction converts the L-shaped structures to X-shaped configurations. (*c*) X-Shaped filament intersections anneal to convert the planar intersections into a three-dimensional structure. X-Shaped polymers colliding with the correct polarity would then produce a three-dimensional network, because actin filaments are helices rotating 360° every 74 nm. To form a three-dimensional structure, sequential unions could anneal in different planes. The precise orientation of the two planar intersections on the annealed filaments would depend on where in the helix turn the junction occurred. This process would offset the two-dimensional perpendicular branching and create a three-dimensional network.

The annealing hypothesis is supported by the actin filament lengths measured within the actin network assembled with actin-binding protein. Since actin-binding protein nucleates

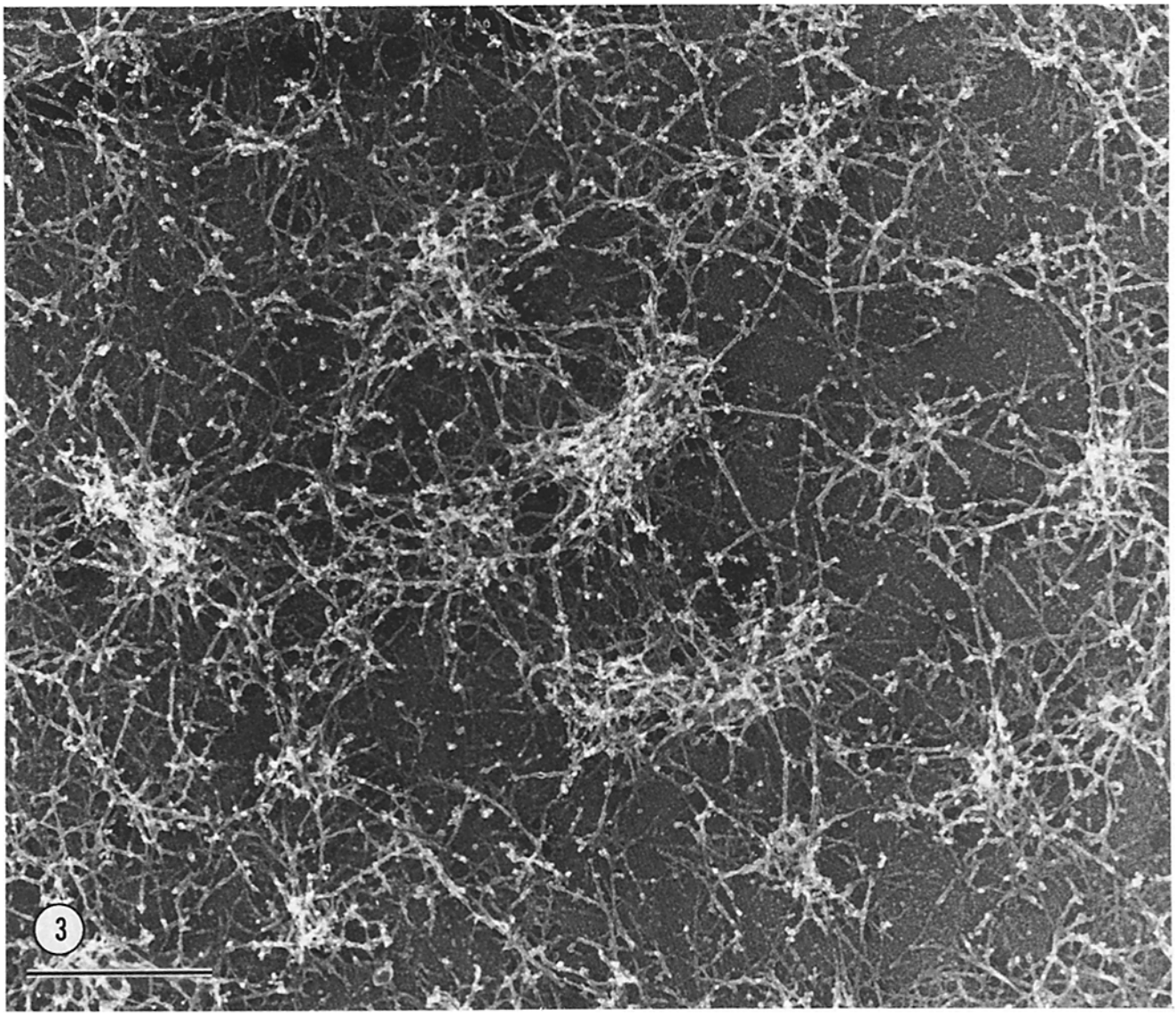


FIGURE 3 Low magnification micrographs of actin assembled in the presence of actin-binding protein at a molar ratio of 1 actin-binding protein to 50 actins. Bar, 1 μm. × 28,000.

actin assembly, it shortens the actin filament length distribution when compared with the same concentration of pure actin by dispersing the available actin into a greater number of filaments (12, 16, 18). At an actin concentration of 1 mg/ml, each molecule of actin-binding protein would nucleate actin filaments 88 and 174 nm in length for the molar ratios of actin-binding protein to actin of 1:25 and 1:50, respectively. However, since actin-binding protein is bivalent, having two domains with binding sites for actin (11), it has two regions that can nucleate filament elongation. Therefore, each actin-binding protein molecule should generate actin filaments 44 and 87 nm in length. Instead, the measured distance between actin filament intersections on the micrographs was approximately twice this predicted value, being 103 and 165 nm at the two actin-binding protein concentrations, respectively. These values are near those predicted if actin-binding protein nucleated only one actin filament. Since each actin-binding protein molecule must nucleate two actin filaments, the simplest explanation for the lengths measured is the annealing of two filaments nucleated by different actin-binding protein molecules.

Although widely accepted as a mechanism for actin filament assembly (18), filament annealing has never been directly established. Therefore, we cannot rule out the possibility that network assembly occurs by way of monomer exchange from the ends of these short actin polymers (19, 21, 30, 32). However, the final attachments of two actin filaments would still require either an annealing event or the simultaneous attachment of one actin monomer onto two actin filaments. Another, more complicated mechanism for forming an intact network would be similar to the one outlined above except that step *c* would be different. In the last scheme, actin-binding protein molecules could join the X-shaped filament fragments together into a network. This mechanism would require the persistence of free molecules of actin-binding protein that did not participate in actin nucleation, which seems unlikely.

## Network Discontinuity

The assembly of actin network in the presence of actin-binding protein is discontinuous. One explanation for this observation is that actin monomers cannot assemble on one area of the grid without decreasing their concentration else-

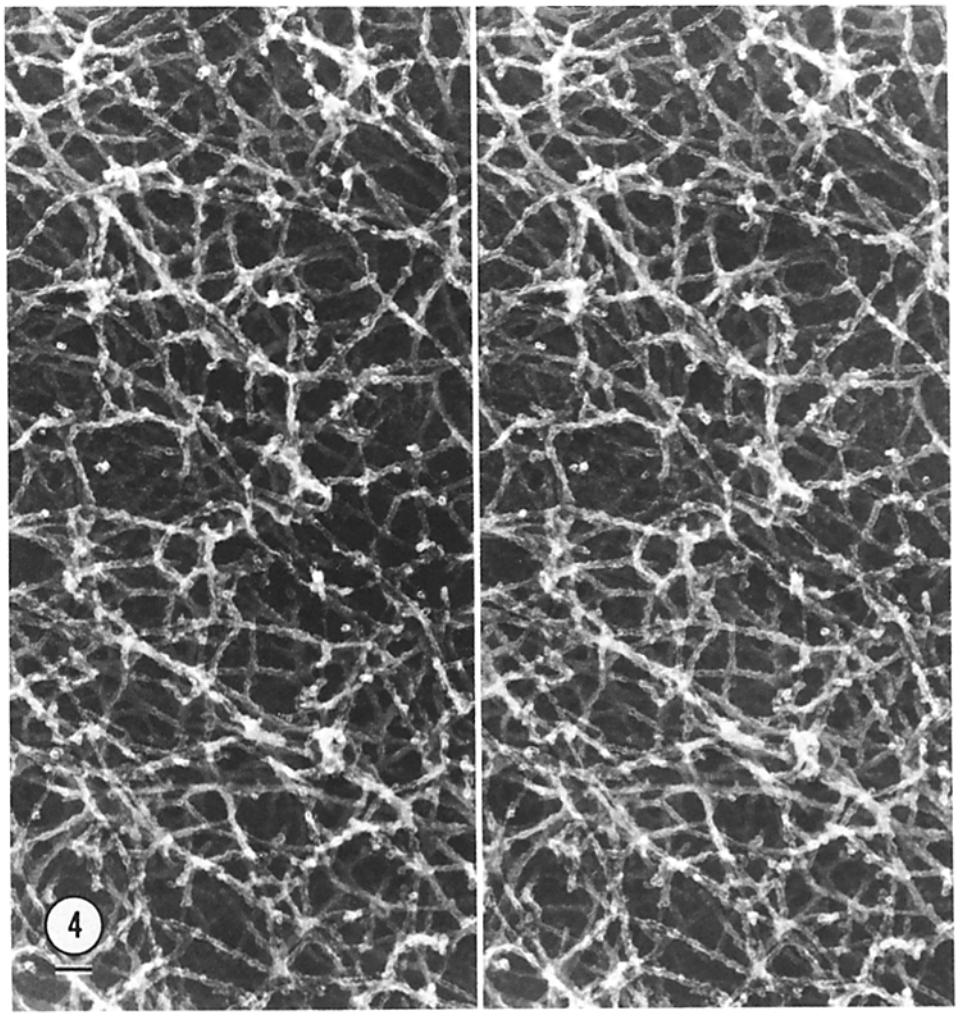


FIGURE 4 Stereo pair electron micrographs of actin plus actin-binding protein at a mole ratio of 50:1. The actin-actin-binding protein mixture forms a branching polymer network in which the actin filaments are short and straight. They have a 10-nm diameter and a helical twist. The average concentration of actin in this micrograph is 7.8 mg/ml. Tilt is ±6°. Bar, 1 μm. × 50,000.

where. The kinetics of actin assembly would accentuate the fluctuation densities of actin monomers initially on the grid surface. We estimated the surface area covered by filament densities in Fig. 3 by cutting out, weighing, and calculating the percent area of the micrograph covered by the densities. Dense regions occupied 30% of the surface area. If these areas contained an average of 6 mg/ml of actin, redistribution of the actin over the surface yields a final concentration of 1.8 mg/ml. This value is a reasonably close approximation to the concentration initially applied to the grid (1 mg/ml).

In contrast to the rheological properties of pure F-actin (36), those of actin assembled with actin-binding protein reflect the presence of strong bonds at actin filament junctions (28). Assuming an assembly of cubes with 100 nm between corners and that share adjoining sides, an actin concentration of 7.8 mg/ml would be required to construct a three-dimensional network consisting of perpendicular intersections, 100 nm apart. This value is within the 6–12 mg/ml range of concentrations measured in the densities on the grids. However, the average actin filament concentration applied to the grids in these experiments was much lower (1 mg/ml), and therefore the entire system could not be expected to behave or look like a gel. Accordingly, concentrations of actin in the 1 mg/ml range assembled with actin-binding protein are more resistant to deformation by stress than an equivalent concentration of pure actin but still exhibit some flow in response to stress (28). Higher concentrations of actin (≥4 mg/ml) are necessary to form networks that cease to flow at all under stress.

## *Relationship to Cell Structure*

One of the most remarkable features of actin-binding protein is its ability to cross-link actin into a perpendicular network that resembles the arrangement of actin filaments in the cortex of mammalian cells. However, many other proteins have been purified and demonstrated to bind and cross-link actin filaments (for reviews, see references 22 and 31). The effect of these additional molecules on actin structure requires investigation. Nevertheless, the preparation of actin networks cross-linked by actin-binding protein represents a first step in reconstructing cytoplasm.

## APPENDIX:

## *A Microcomputer Method for Analyzing Three-dimensional Networks in Stereo Micrographs*

In this appendix, a program for a microcomputer system is described that calculates three-dimensional information from stereo photographs. Straight line segments of filaments on each photograph are entered into a microcomputer by means of a graphic tablet. The two-dimensional data obtained from each micrograph are then manipulated by the computer to yield the following three-dimensional information: lengths of filaments, their relative heights, and the angles formed by filaments that intersect. The concentration of actin in a defined volume can also be calculated.

### *Height*

The third dimension of each point is obtained from the stereo pair, knowing the tilt angle ($\theta$) of the specimen when photographed, the magnification ($M$), and

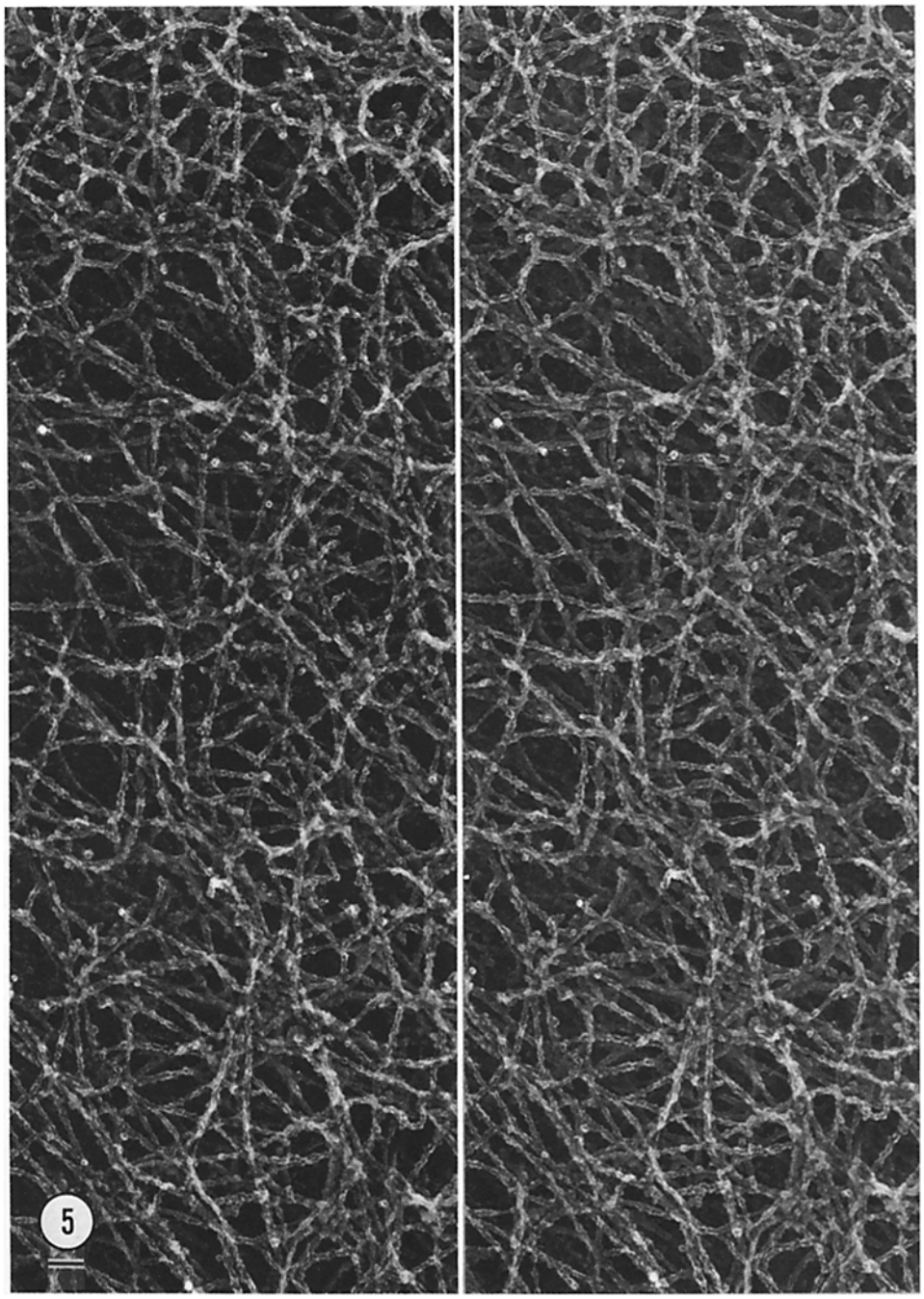


FIGURE 5 Stereo pair electron micrographs of actin-actin-binding mixtures of a mole ratio of 25:1. The actin network has tightened compared to the network seen at a mole ratio of 50:1. However, the actin filaments retain their morphological appearance and perpendicular branching. The average concentration of actin in these micrographs is 11.1 mg/ml. Stereo pairs taken at ±6°. Bar, 1 μm. × 50,000.

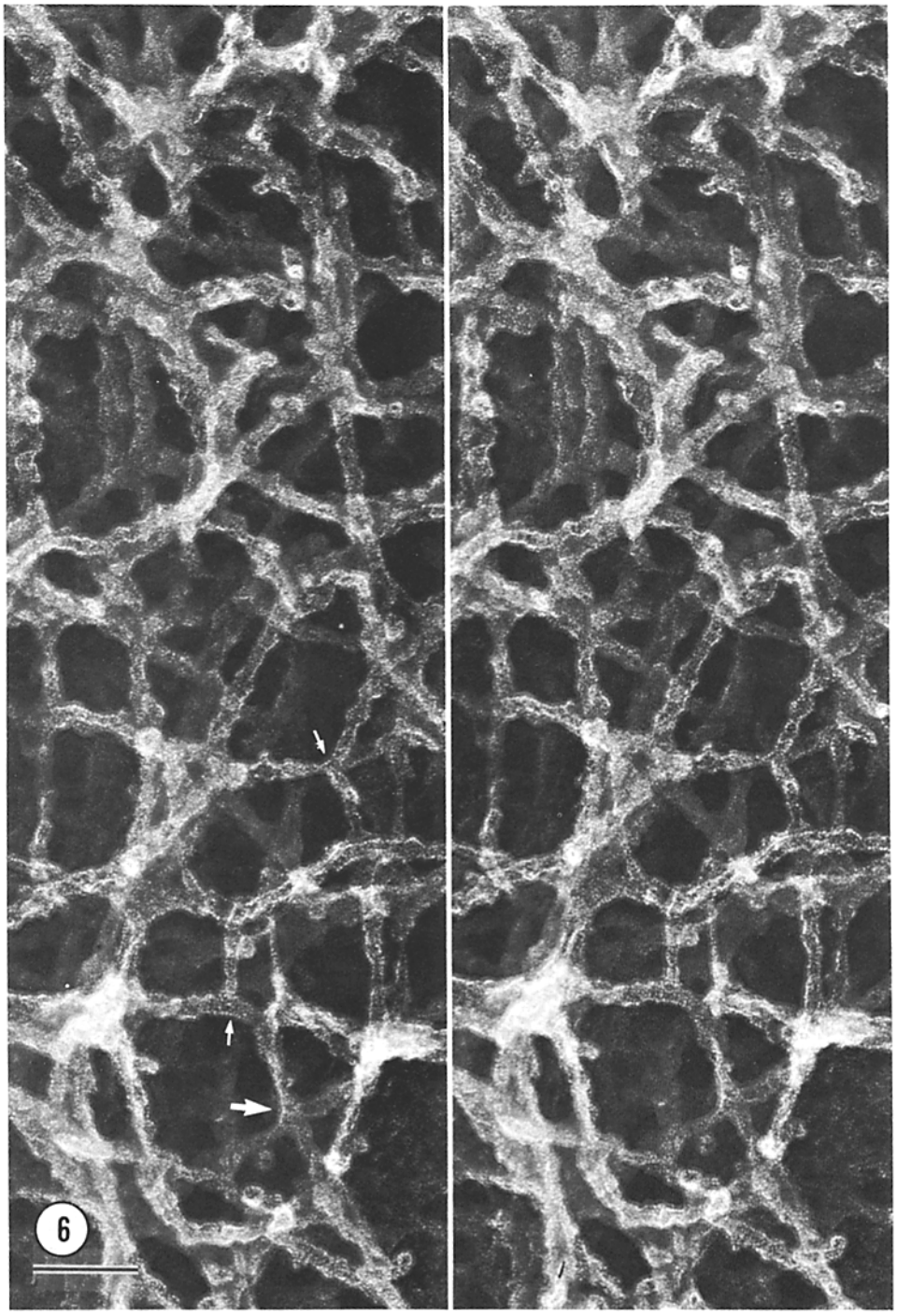


FIGURE 6 High magnification stereo micrographs of actin–actin-binding protein mixtures of a mole ratio of 50:1. The small arrows indicate branches designated in the text as T- or Y-junctions. The large arrows indicate X-junctions. Bar, 100 nm. × 150,000.

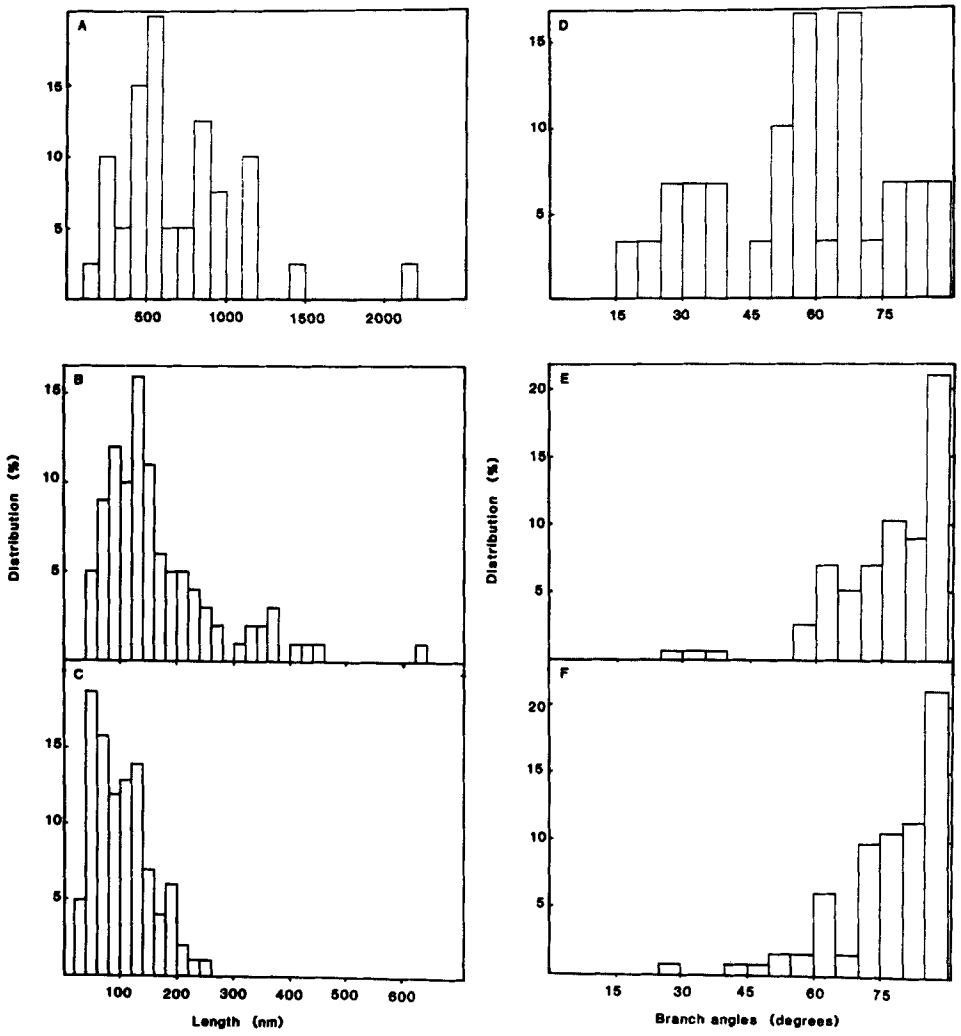


FIGURE 7 Histograms showing the distance between filament intersections (*A*, *B*, and *C*) and distributions for the angle of filament branching (*D*, *E*, and *F*). Actin (*A* and *D*), actin-binding protein:actin in a mole ratio of 1:50 (*B* and *F*) and 1:25 (*C* and *F*). The number average length ± SD of the filament intersections in *A*, *B*, and *C* was 695 ± 380 nm, 166 ± 102 nm, and 103 ± 50 nm, respectively, where $n = 100$. The average angle was not calculated. However the angle of intersection for actin appears to vary continuously between 15° and 90°. In contrast, for actin copolymerized with actin-binding protein the angle of intersection approaches 90°.

the parallax distance ($P$). The parallax distance is the apparent horizontal distance traveled by the point when comparing the paired photographs. The parallax distance is calculated by the computer using identical reference points entered from each photograph of the stereo pair. As shown in Fig. 9, the height ($h$) of point $A$ is

$$h = s/\sin\theta. \tag{1}$$

Since, as defined in Fig. 9, $P = 2s$, the height of point $A$ is

$$h = (P \times M)/(2 \sin\theta). \tag{2}$$

In the following description, the heights of points *1* and *2* in the model of Fig. 10 will be calculated. In this example, the graphics tablet is oriented under the photographs such that the origin of the $X$ axis and $Y$ axis is at the lower left corner of the figure. The units used in this example are arbitrary. First, the same reference point (*arrows*) is selected for each photograph. The ($X$, $Y$) coordinates of the reference point in the left ($L$) photograph are (37, 8), and in the right ($R$) photograph they are (102, 8). Points *1* and *2* have $L$ ($X$, $Y$) coordinates of (20, 52) and (37, 52), respectively. The $R$ ($X$, $Y$) coordinates are (82, 52) and (102, 52), respectively. Point *1* is, thus, 37–20 or 17 U to the left of the reference point in $L$, and 102–82 or 20 U to the left of the reference point in $R$. Point *2* has not moved relative to the reference points. The parallax distance of point *1* is the difference between these two values or 20–17, which equals 3. For point 2, it is 0. These points can be converted directly to heights by Eq. 2 once the magnification is determined. In this case, the length of the only vertical stick on the model was 15 cm. The length determined from the figure is 52–12 U or 40 U. Therefore, the magnification is 15 cm/40 U or 0.375 cm/U. The height of point *1* is (3 × 0.375 cm)/(2 × sin 6°) or 5.34 cm. The height of point *2* is therefore 0.

## Distances and Angles

LINE LENGTH: Each point recorded is stored as a set of $X$, $Y$, $Z$ coordinates where the $X$ and $Y$ values are taken from the left-hand stereo picture and the $Z$-value is taken from the calculated height. Lines are defined by two points entered sequentially. An array of 20 lines, dimensioned as $L(20, 2, 3)$, required 120 numbers (1.2 K bytes) to be stored in memory. The calculated length of a line is determined from the Pythagorean formula in solid space:

$$L = \sqrt{(X_2 - X_1)^2 + (Y_2 - Y_1)^2 + (Z_2 - Z_1)^2}. \tag{3}$$

The actual lengths are computed based on the magnification of the photomicrograph.

The length of the line connecting points *1* and *2* in Fig. 10 was calculated. The $X$, $Y$, $Z$ coordinates were first converted to centimeters (actual lengths in the photographs). The length, therefore, according to Eq. 3 is $((0–6.45)^2 + (17.3–17.3)^2 + (0–5.34)^2)^{1–2}$ or 8.36 cm.

INTERSECTION ANGLE: The following geometric formulas were utilized to determine whether lines crossing in space touched, and if so, the angle at which they intersect.

The distance between lines $P_1P_2$ and $P_3P_4$ (Fig. 11) is defined as the length of the line segment $d$ which is perpendicular to both lines. The direction of this line segment is found from the vector cross product:

$$\mathbf{V} = \mathbf{P_1P_2} \times \mathbf{P_3P_4}$$

The length of line segment $d$ is the projection of any line connecting the two lines (such as the line between $P_1$ and $P_3$ in Fig. 11) onto this perpendicular vector. The length is obtained as the absolute value of the dot product of the line $P_1P_3$ and the unit vector $\mathbf{V}/\mathbf{V}$ or:

$$d = \mathbf{P_1P_3} \cdot [(\mathbf{P_1P_2} \times \mathbf{P_3P_4})/(|\mathbf{P_1P_2} \times \mathbf{P_3P_4}|)].$$

The angle between the two lines (or cellular elements) is found using the dot product formula which is defined as:

$$\mathbf{V_1} \cdot \mathbf{V_2} = |\mathbf{V_1}| \cdot |\mathbf{V_2}| \cos\theta.$$

Rearranging, we have:

$$\cos\theta = (\mathbf{V_1} \cdot \mathbf{V_2})/(|\mathbf{V_1}| \cdot |\mathbf{V_2}|).$$

Where the two lines are defined by the four points $X(1–4)$, $Y(1–4)$, $Z(1–4)$, the right side of the equation is found as:

$$\mathbf{V_1} \cdot \mathbf{V_2} = (X_2–X_1)(X_4–X_3) + (Y_2–Y_1)(Y_4–Y_3) + (Z_2–Z_1)(Z_4–Z_3)$$

$$|\mathbf{V_1}| = \sqrt{(X_2–X_1)^2 + (Y_2–Y_1)^2 + (Z_2–Z_1)^2}$$

$$|\mathbf{V_2}| = \sqrt{(X_4–X_3)^2 + (Y_4–Y_3)^2 + (Z_4–Z_3)^2}.$$

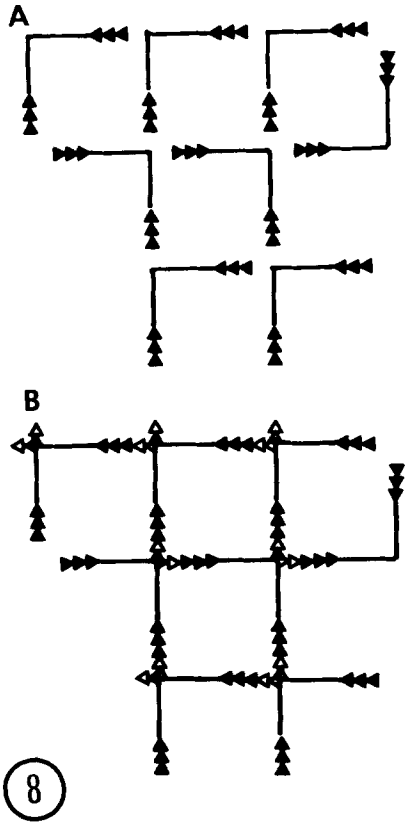


FIGURE 8 Model for assembly of a gel network by filament reannealing. *(A)* Initial preferred end assembly of chain on the two binding sites of actin-binding protein forms L-shaped polymer fragments. Actin-binding protein is as the vertex of the L, and actin is indicated by the solid triangles. The polarity of the filaments is indicated by the orientation of the triangles. *(B)* With time, elongation also occurs on the non-preferred end of the filaments as indicated by the open triangles. This forms T- or X-shaped fragments which can then anneal.

Since it may not be clear from visual inspection of stereo micrographs whether the two elements actually intersect, it has been convenient to have access to the calculated distance between them. If the distance is zero or within an expected amount of experimental error, the intersection angle is retained as valid. When the distance between lines is >0, the angle calculated is the angle of one line crossing over the other when viewed looking down on the elements (at a perpendicular vector from the elements).

## Concentrations

The total length of all the elements in a defined volume of rectangular three-dimensional space can be summed from the lengths of the individual elements in this space. The volume is defined by indicating the desired rectangular area on the graphics tablet with the pen. The computer lists on the monitor the heights of the lowest and highest elements. The operator then enters the height of the lower boundary and the thickness of the desired volume. The lengths of all the elements traversing within the chosen boundaries of the volume are summed. The program finds the points of intersection of each individual element with the faces of the rectangular volume. For example, as illustrated in Fig. 12 the length of the element to be calculated is $P_1P_2$. The working area is from XW to XE and from YN to YS. Points $P_1$ and $P_2$ are outside the defined rectangular volume. New points, $Q_1$ and $R_2$, need to be calculated so that segment $Q_1R_2$ will be taken as the length of the element in the volume. Point $Q_1$ is determined first. The $X$, $Y$, $Z$ components of it are:

$$XQ_1 = XW$$

$$YQ_1 = (XW - X_1)/(X_2–X_1) \times (Y_2 - Y_1) + Y_1$$

$$ZQ_1 = (XW - X_1)/(X_2–X_1) \times (Z_2 - Z_1) + Z_1.$$

A similar calculation is required for $R_2$, since the point $P_2$ is higher than the

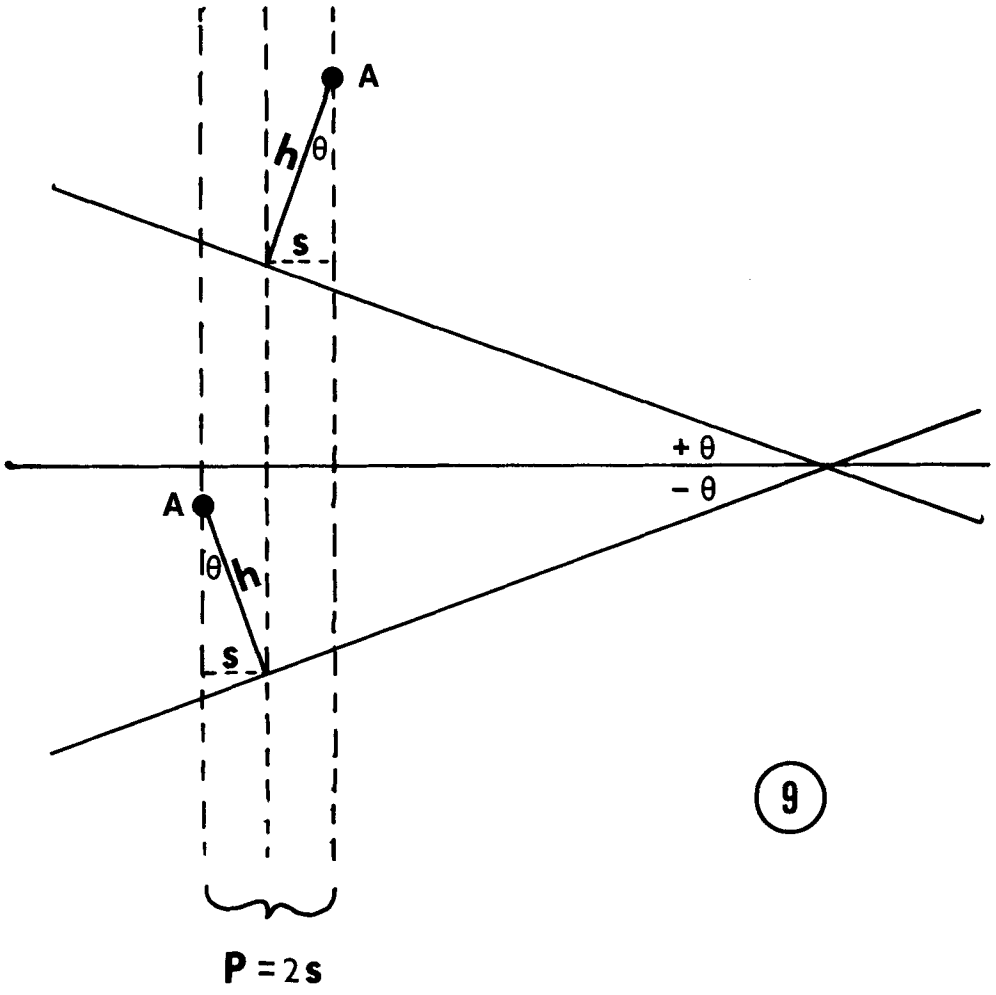


FIGURE 9 An object at a height of $h$ on a surface will appear to travel a horizontal distance of $P = 2S$ after tilting the specimen from $\theta°$ below the horizontal to $\theta°$ above.

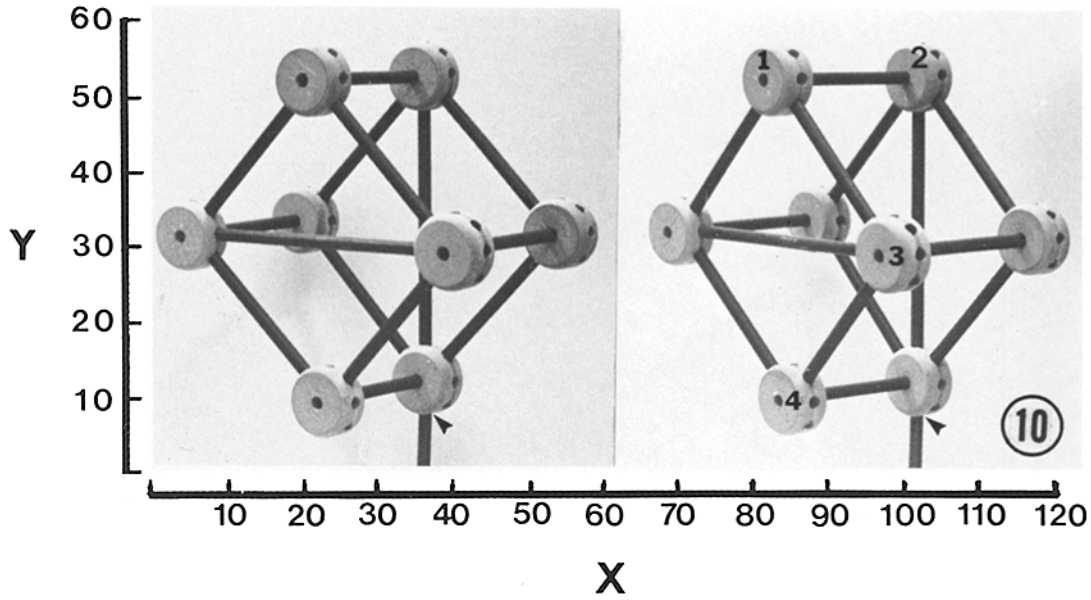


FIGURE 10 Stereo photographs of the stick model. The second photograph was taken after ±6° of horizontal rotation of the model to generate the stereo pair.

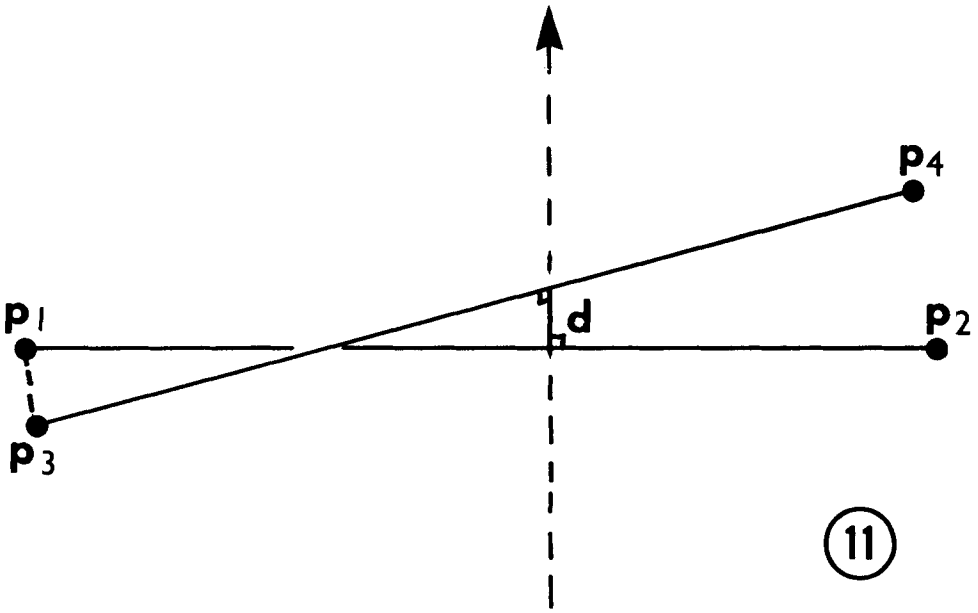


FIGURE 11 The length of line segment $d$ is calculated as the dot product of the vector $P_1P_3$ and the vector perpendicular to the two nonintersecting line segments $P_1P_2$ and $P_3P_4$.

defined volume which extends only from $Z = 0$ to $Z = TP$. The components of $R_2$ are calculated as:

$$XR_2 = (TP - Z_1)/(Z_2 - Z_1) \times (X_2 - X_1) + X_1$$

$$YR_2 = (TP - Z_1)/(Z_2 - Z_1) \times (Y_2 - Y_1) + Y_1$$

$$ZR_2 = TP.$$

Now the desired length of line $P_1P_2$ within the chosen volume can be calculated as the line segment $Q_1R_2$ as follows:

$$\text{Length} = \sqrt{(XR_2 - XQ_1)^2 + (YR_2 - YQ_1)^2 + (ZR_2 - ZQ_1)^2}.$$

After all line segments are summed up, a concentration can be calculated if desired.

## Testing the Program

A stick model was prepared (Fig. 10) to validate the computer program with an object of known dimensions. Measurements were made of the length between intersection points, using a ruler. Except for the two diagonal sticks, all of the connecting elements were perpendicular to each other. This model was photographed at $a \pm 6°$ of rotation to produce the stereo photographs used on the graphics tablet. The microcomputer program was applied to the stick model shown in the stereo photographs of Fig. 10.

## Length

Three sets of elements in the stick model were measured. The eight connecting sticks of the front and back faces of the model measured 10.6 ± 0.2 cm (mean ± SD) by ruler and 10.8 ± 0.5 cm by the computer. These were not statistically different ($P > 0.2$). The four elements that connected the two faces of the model measured 7.85 ± 0.2 cm by ruler and 8.31 ± 1.1 cm by the computer. These were also not statistically different ($P > 0.2$). Each of the two diagonal elements measured 15.0 cm by ruler and 15.2 ± 1.3 cm (16.2 and 14.3 cm) by the computer.

## Angles

The 24 perpendicular angles at the eight corners of the cube were assumed to be 90° and the angles formed by the two diagonal elements were assumed to be

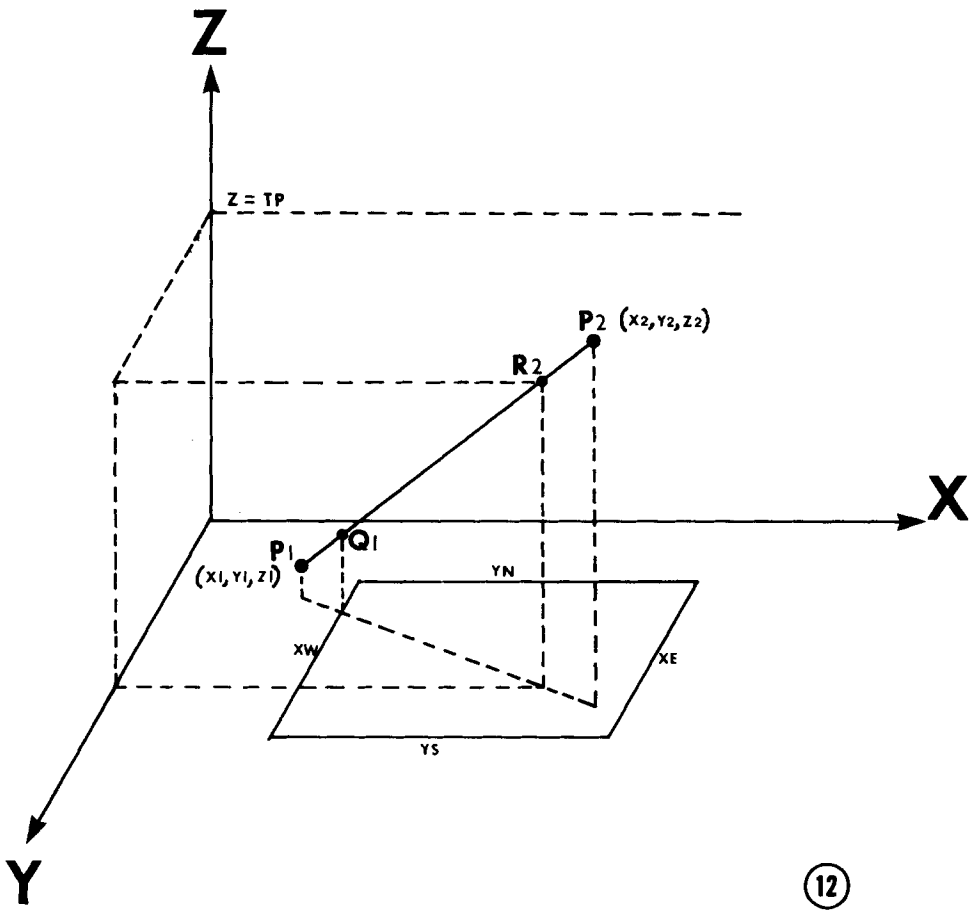


FIGURE 12 Diagram illustrating that the portion of line $P_1 P_2$ within the rectangular volume of area *XW, XE, YN, YS* and height $Z = 0$ to $Z = TP$ is line segment $Q_1 R_2$.

45°. The computer determined the perpendicular angles to be 90.2 ± 5.0° with a range of 80.3–100.9°. The angles of intersection of the diagonal elements in the corners were calculated as 45.4 ± 2.3° with a range of 41.0–47.2°. The angle and distance between the two diagonal nonintersecting elements were calculated to be 89.8° and 7.87 cm, respectively. The actual distance measured was 7.85 cm.

## Concentrations

Since the concentrations are not applicable to the stick model, we determined the total length of the stick elements for the volume of the model. The sum of all the sticks in the model was determined to be 150 cm by the computer and 146 cm with the ruler.

To check the serial sectioning subprogram, we arbitrarily divided the model into two sections. The total sum of the length of the sticks in the two pieces should therefore add up to 150 cm. When the model was divided 9 cm up from its back corner, the lower part contained a total length of 91.2 cm and the upper part 58.8 cm. Similarly, when it was divided near vertical, the right side contained a total length of 72.5 cm and the left side 79.2 cm. A precise fragment was defined by cutting a section through the model (Fig. 10) that included only the sticks from point *1* to *3* and from point *3* to *4* and the right half of the horizontal stick cut off by an imaginary line from point *1* to *4*. The sum of these lengths was 29.2 cm by the computer and 28.3 cm by ruler.

We thank Tom Stossel and Ken Zaner for their encouragement, helpful discussion, and insight.

This work was supported by grants from the U. S. Public Health Service (HL 27971, HL 19429, DE 06540, and DE 06123), the Council for Tobacco Research (11116), the Edwin S. Webster Foundation, and the Veterans Administration.

*Received for publication 12 July 1982, and in revised form 24 January 1983.*

## REFERENCES

1. Anderson, T. 1951. Techniques for the preservation of the three-dimensional structure in preparing specimens for the electron microscope. *Trans. N. Y. Acad. Sci. Ser. II* 13:130–134.
2. Boyles, J., and D. F. Bainton. 1979. Changing patterns of plasma membrane-associated filaments during the initial phases of polymorphonuclear leukocyte adherence. *J. Cell Biol.* 82:347–368.
3. Bretscher, A. 1981. Fimbrin is a cytoskeletal protein that crosslinks F-actin *in vitro*. *Proc. Natl. Acad. Sci. USA.* 78:6849–6853.
4. Bretscher, A., and K. Weber. 1980. Villin is a major protein of the microvillus cytoskeleton which binds both G and F actin in a calcium-dependent manner. *Cell.* 20:839–847.
5. Brotschi, E. A., J. H. Hartwig, and T. P. Stossel. 1978. The gelation of actin by actin-binding protein. *J. Biol. Chem.* 253:8988–8993.
6. Bryan, J., and R. E. Kane. 1978. Separation and interaction of the major components of sea urchin actin gel. *J. Mol. Biol.* 125:207–224.
7. Buckley, I. K., and K. R. Porter. 1967. Cytoplasmic fibrils in living culture cells. *Protoplasm.* 64:349–362.
8. Buckley, I. K., and K. R. Porter. 1975. Electron microscopy of critical pointed dried cultured cell. *J. Microsc. (Oxf.).* 104:107–120.
9. Flory, P. J. 1956. *Proc. R. Soc. Lond. B. Biol. Sci.* A234:60.
10. Glenney, J. R., P. Kaulfus, P. Matsudaira, and K. Weber. 1981. F-actin binding and bundling properties of fimbrin, a major cytoskeletal protein of microvillus core filaments. *J. Biol. Chem.* 256:9283–9288.
11. Hartwig, J. H., and T. P. Stossel. 1981. The structure of actin-binding protein molecules in solution and interacting with actin filaments. *J. Mol. Biol.* 145:563–581.
12. Hartwig, J. H., J. Tyler, and T. P. Stossel. 1980. Actin-binding protein promotes the bipolar and perpendicular branching of actin filaments. *J. Cell Biol.* 87:841–848.
13. Heuser, J. E., and M. W. Kirschner. 1980. Filament organization revealed in platinum replicas of freeze-dried cytoskeletons. *J. Cell Biol.* 86:212–234.
14. Hirokawa, N., and J. E. Heuser. 1981. Quick freeze, deep-etch visualization of the cytoskeleton beneath surface differentiations of intestinal epithelial cells. *J. Cell Biol.* 91:399–404.
15. Deleted in press.
16. Kawamura, M., and K. Maruyama. 1970. Electron microscopic particle length of F-actin polymerized *in vitro*. *J. Biochem.* 67:437–457.
17. Margaritis, I. H., A. Elgasaeter, and D. Branton. 1977. Rotary replication for freeze-etching. *J. Cell Biol.* 74:47–56.
18. Oosawa, F. 1970. Size distribution of protein polymers. *J. Theor. Biol.* 27:69–86.
19. Pardee, J. D., P. A. Simpson, L. Stryer, and J. A. Spudich. 1982. Actin filaments undergo limited subunit exchange in physiological salt conditions. *J. Cell Biol.* 94:316–324.
20. Pollard, T. D., U. Aebi, J. A. Cooper, W. E. Fowler, and P. Tseng. 1981. Actin structure, polymerization, and gelation. *Cold Spring Harbor Symp. Quant. Biol.* 46:513–524.
21. Pollard, T. D., and M. S. Mooseker. 1981. Direct measurement of actin polymerization rate constants by electron microscopy of actin filaments nucleated by isolated microvillus cores. *J. Cell Biol.* 88:654–659.
22. Schliwa, M. 1981. Proteins associated with cytoplasmic actin. *Cell.* 25:587–590.
23. Schliwa, M., and J. van Blerkom. 1981. Structural interaction of cytoskeletal components. *J. Cell Biol.* 90:222–235.
24. Schliwa, M., J. van Blerkom, and K. R. Porter. 1981. Stabilization of the cytoplasmic ground substance in detergent-opened cells and a structural and biochemical analysis of its composition. *Proc. Natl. Acad. Sci. USA.* 78:4329–4333.
25. Small, J. V. 1981. Organization of actin in the leading edge of cultured cells: influence of

osmium tetraoxide and dehydration on the ultrastructure of actin networks. *J. Cell Biol.* 91:695–705.
26. Spudich, J. A., and S. Watt. 1971. The regulation of rabbit skeletal muscle contraction. I. Biochemical studies of the interaction of the tropomyosin-troponin complex with actin and the proteolytic fragments of myosin. *J. Biol. Chem.* 246:4866–4871.
27. Stossel, T. P., and J. H. Hartwig. 1976. Interaction of actin, myosin and a new actin-binding protein of rabbit pulmonary macrophages II. Role in cytoplasmic movement and phagocytosis. *J. Cell Biol.* 68:602–614.
28. Stossel, T. P., J. H. Hartwig, H. L. Yin, K. S. Zaner, and O. I. Stendahl. 1982. Actin gelation and the structure of cortical cytoplasm. *Cold Spring Harbor Symp. Quant. Biol.* 46:569–578.
29. Takebayashi, T., Y. Morita, and F. Oosawa. 1977. Electron microscopic investigation of the flexibility of F-actin. *Biochim. Biophys. Acta.* 492:357–363.
30. Wang, Y., and D. L. Taylor. 1981. Probing the dynamic equilibrium of actin polymerization by fluorescence energy transfer. *Cell.* 27:429–436.
31. Weeds, A. 1982. Actin-binding proteins—regulators of cell architecture and motility. *Nature (Lond.).* 296:811–816.
32. Wegner, A. 1976. Head to tail polymerization of actin. *J. Mol. Biol.* 108:139–150.
33. Wolosewick, J. J., and K. R. Porter. 1979. Microtrabecular lattice of the cytoplasmic ground substance. Artifact or reality. *J. Cell Biol.* 82:114–139.
34. Woodrum, D. T., S. A. Rich, and T. D. Pollard. 1975. Evidence for biased bidirectional polymerization of actin filaments using heavy meromyosin prepared by an improved method. *J. Cell Biol.* 67:231–237.
35. Zaner, K., and T. P. Stossel. 1982. Some perspectives on the viscosity of actin filaments. *J. Cell Biol.* 93:987–991.
36. Zaner, K., and T. P. Stossel. 1983. Physical basis of the rheologic properties of actin filaments. *J. Biol. Chem.* In press.